Chapter 7

Effect of electropulsing on martensite

7.1 Introduction

Martensitic steels often undergo a secondary treatment called tempering to enhance certain mechanical properties. Tempering involves distinct stages, each contributing to specific microstructural modifications, as elaborated in Section 1.5.6. During tempering, the material is subjected to prolonged exposure to heat (typically 1 hour), which leads to softening due to carbon rejection from the martensite phase [113] .

In the current Chapter, the focus lies on a low alloy, high carbon steel with coexisting martensite and austenite phases, developed through tailored heat treatment methods outlined in the experimental section. Subsequently, electropulsing is applied at various current densities to induce further changes in the microstructure of both the martensite and austenite phases, as well as alterations in hardness value.

7.2 Results

The D2 steel, which was previously austenitized and air-cooled to room temperature (D2-A), undergoes electropulsing treatment. The EP parameters are provided in Table 2.2 of the experimental Section. The samples are electropulsed both at a high current density of 8.8 kA/mm^2 (D2-A-EP-1) and a low current density of 4.8 kA/mm^2 (D2-A-EP-1-LCD). The calculated temperature rise in the high current density sample is approximately 1230 °C, while in the low current density sample it is around 290 °C.

An optical micrograph of the D2-A sample reveals the presence of lenticular martensite (α_m) and RA as shown in Figure 7.1a. The lenticular morphology of martensite is also clearly observed in the SEM-SE image (Figure 7.1b). The EBSD-IQ map of the D2-A sample, depicted in Figure 7.1c, shows bright strain-free regions corresponding to the austenite phase and grey regions with higher strain corresponding to the martensite phase. This correlation is further confirmed by comparing the IQ map with the phase map shown in Figure 7.2c. The analysis

indicates that the amount of martensite is approximately 54 percent, with the rest being retained austenite.

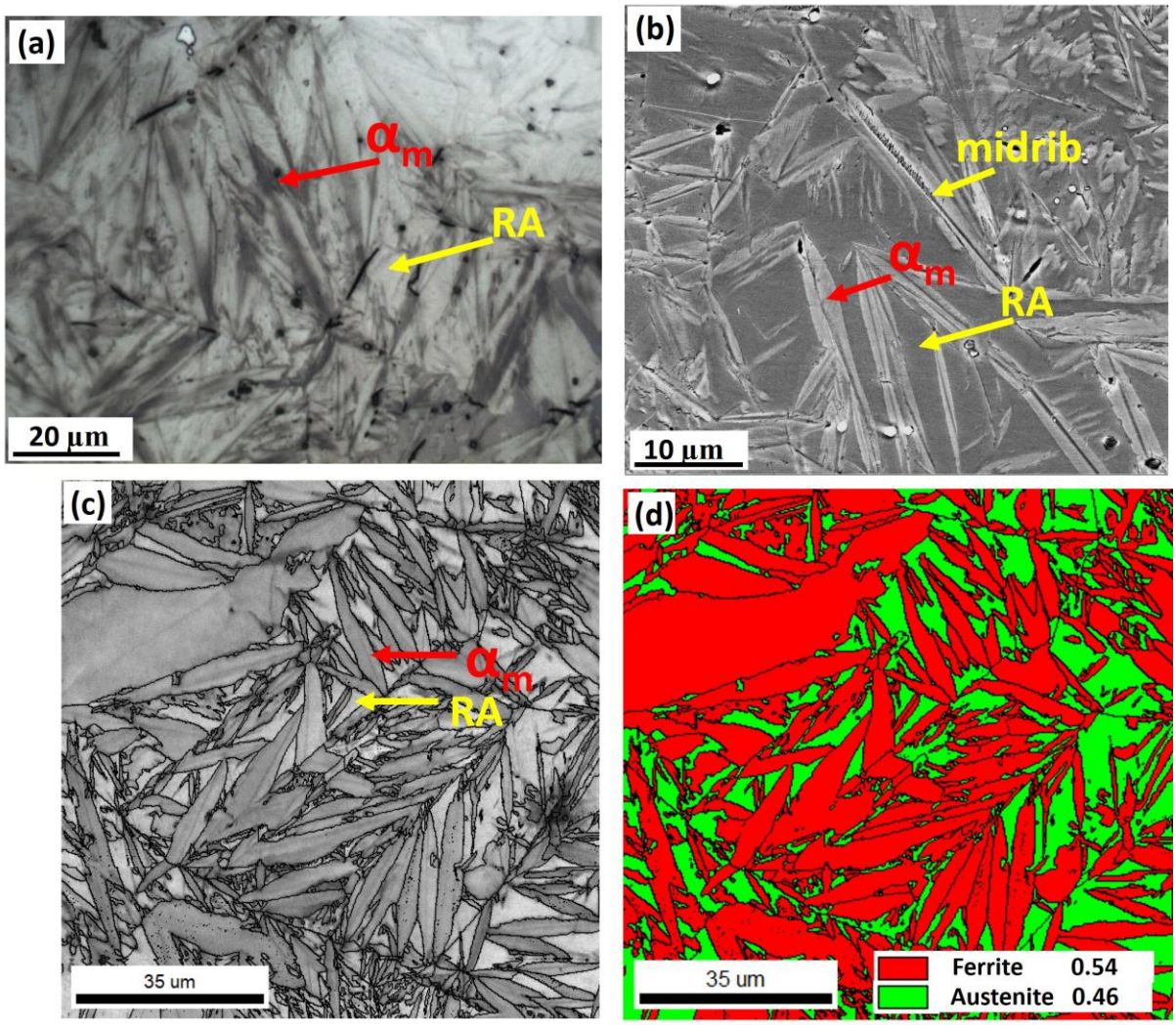

Figure 7.1. *Micrographs of D2-A sample (a) Optical, (b) SEM-SE, (c) IQ map and (d) phase map. (α_m and RA denote martensite and retained austenite respectively)*

The EP of the D2-A sample at higher current density (D2-A-EP-1) and lower current density (D2-A-EP-1-LCD) displays lenticular martensite and RA respectively, as shown in the optical micrographs in Figures 7.2a and b. The SEM-SE image of the D2-A-EP-1 sample (Figure 7.2c) reveals two different types of martensite. The deeply etched martensite, designated as α_m, is inherited from the D2-A sample and shows carbide precipitation inside it. The second type of martensite, designated as α'_m is freshly formed and lightly etched.

Additionally, plate-shaped bainite is observed in the microstructure. The bainite phase shows no significant carbide precipitation since it is freshly formed.

In contrast, distinguishing between bainite and martensite is challenging in the D2-A-EP-1-LCD sample as no significant carbide precipitation is observed in the martensite (Figure 7.2d). However, some plate-shaped features are still visible in the micrograph resembling the formation of bainite.

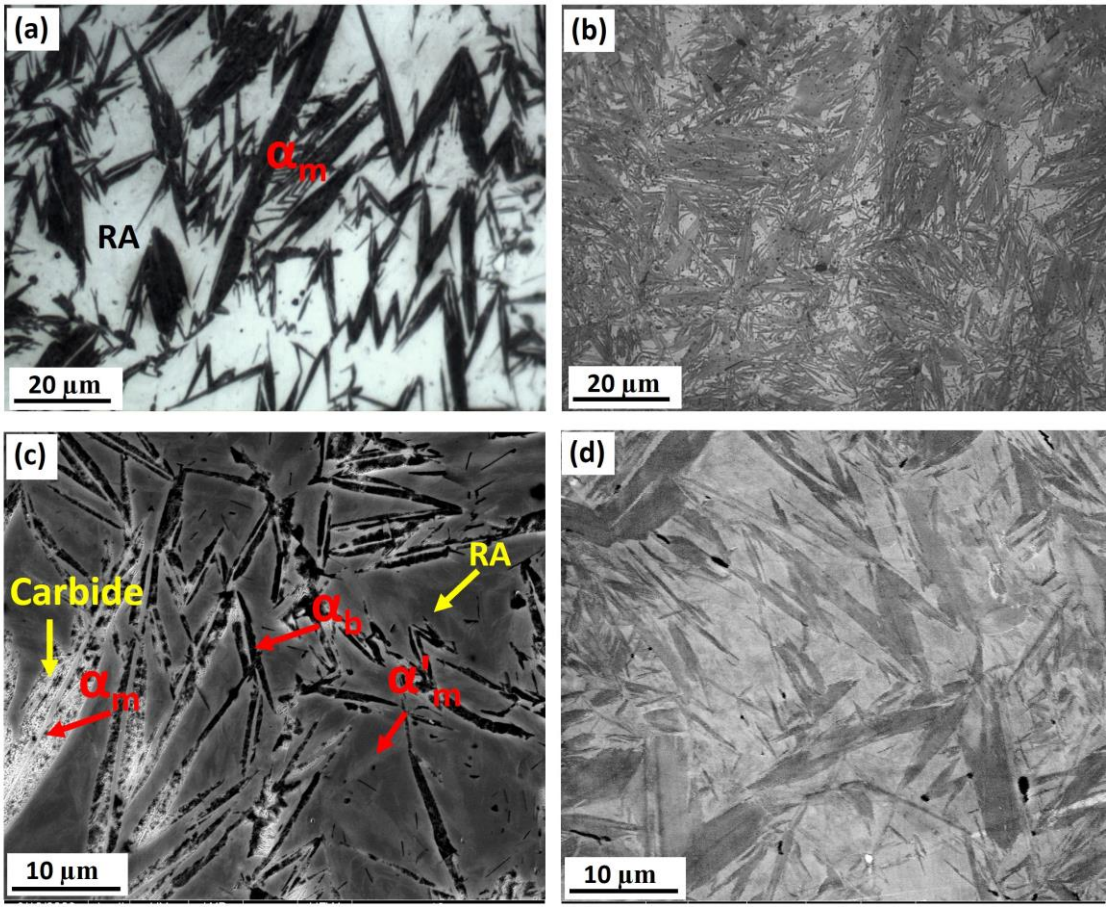

Figure 7.2. *Optical micrographs of (a) D2-A-EP-1, (b) D2-A-EP-1-LCD and SEM-SE images of (c) D2-A-EP-1, (d) D2-A-EP-1-LCD samples.*

The IQ map of the D2-A-EP-1 sample (Figure 7.3a) shows both strained (grey coloured) and strain-free regions (white colour). Austenite is generally less strained compared to bainite and martensite, but the micrograph is observed to consist bainite/martensite having strained and strain-free regions. The strain-free (bright colour) regions are martensite which is

inherited from the initial pre-pulsed sample and strained regions (grey colour) are freshly formed martensite/bainite. The corresponding phase map in Figure 7.3c shows that the fraction of martensite/bainite has increased from the 54% in the D2-A sample to 78% after EP. Although phase quantification using EBSD has some limitations due to its localized information and difficulty in detecting fine carbides, it can be clearly inferred that part of austenite has converted into martensite/bainite through EP.

In the case of low current density sample (D2-A-EP-1-LCD), the IQ map (Figure 7.3d) shows more grey regions, which means presence of high amount of strain. The corresponding phase map (Figure 7.3d) shows that martensite/bainite fraction is 62% and the rest are RA.

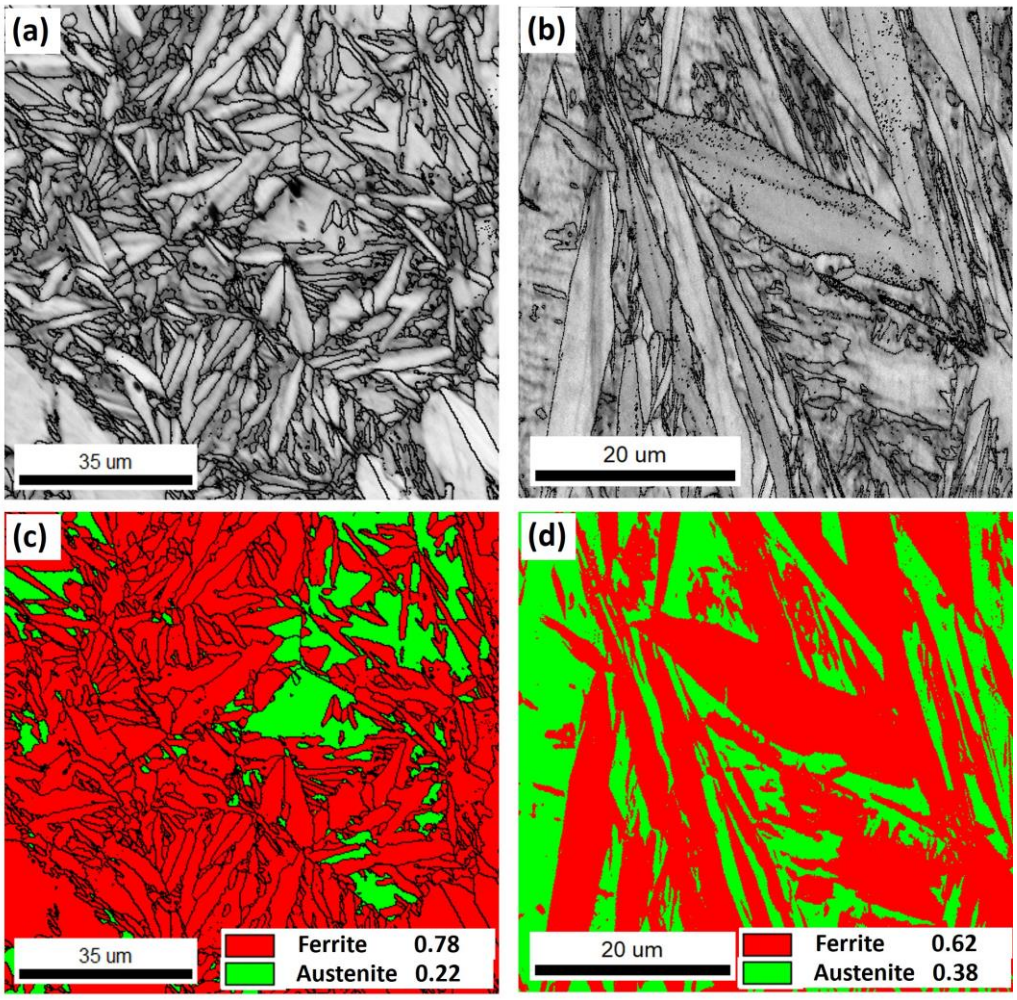

***Figure 7.3**. EBSD-IQ maps of (a) D2-A-EP-1, (b) D2-A-EP-1-LCD and phase maps of (c) D2-A-EP-1, (d) D2-A-EP-1-LCD samples.*

In the D2-A sample (Figure 7.4a), the martensite phase exhibits only 10% of high-angle grain boundaries, with the majority of boundaries being low-angle grain boundaries. After electropulsing treatment (D2-A-EP-1) (Figure 7.4b), the amount of HAGB increases to 35%. Similar observations can be made in the austenite phase, where only 3% of HAGB are present in the D2-A sample (Figure 7.4c), with majority of the boundaries having misorientation angles below 15º. After electropulsing, the amount of HAGB in austenite increases to 16%, and the remaining boundaries are LAGB. However, in the low current density sample (D2-A-EP-1-LCD), the HAGB fraction is similar to that of the D2-A sample in both the martensite (Figure 7.4c) and austenite phases (Figure 7.4f).

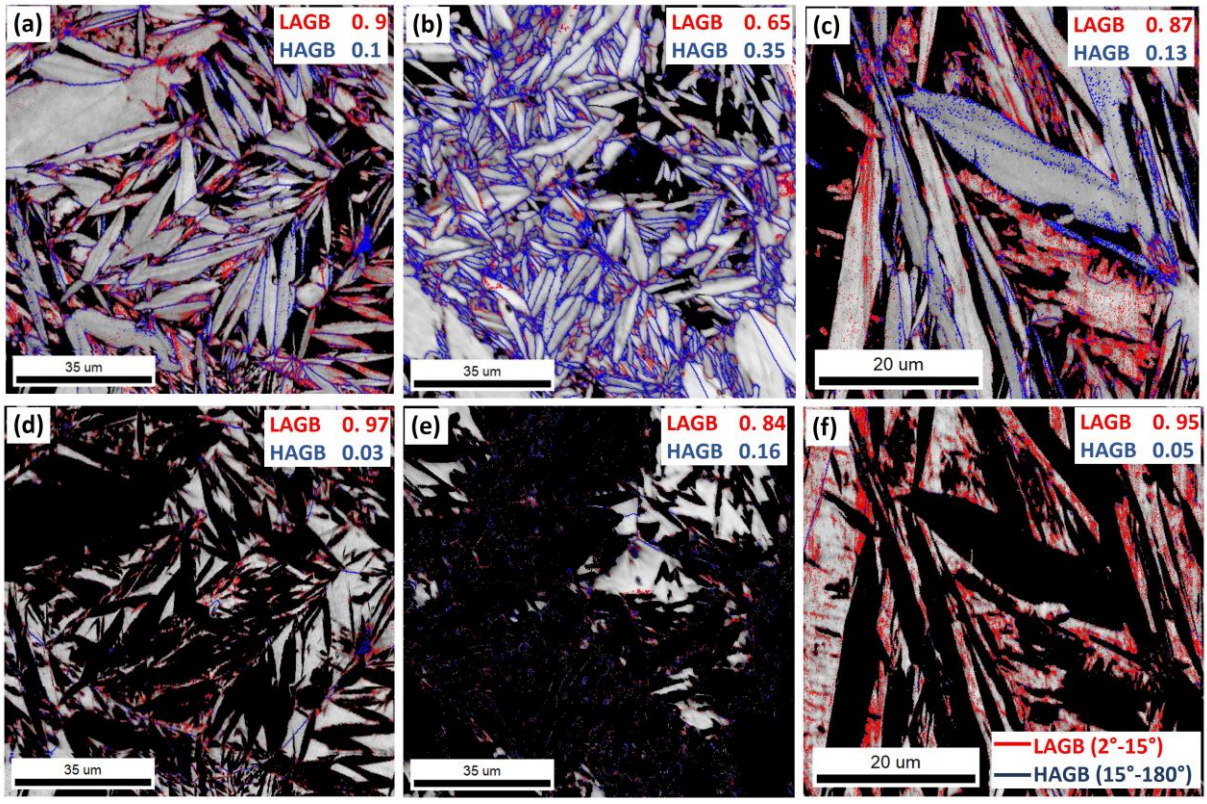

Figure 7.4. *Grain boundaries are superimposed in IQ maps of bainite (a) D2-A, (b) D2-A-EP-1 and (c) D2-A-EP-1-LCD and retained austenite (d) D2-A, (e) D2-A-EP-1 and D2-A-EP-1-LCD.*

The Kernel average misorientation maps of the martensite/bainite and austenite phases are shown in Figure 7.5. In the D2-A sample (Figure 7.5a), the martensite phase exhibits

an average KAM value of 0.78°, which decreases to 0.53° after electropulsing treatment (D2-A-EP-1), indicating the annihilation of dislocations. A similar trend is observed in the austenite phase, where the initial KAM value was 0.67° (Figure 7.5d), and after electropulsing (D2-A-EP-1), it decreases to 0.5° (Figure 7.5e). However, in the low current density sample (D2-A-EP-1-LCD), both the martensite/bainite (Figure 7.5c) and retained austenite phases (Figure 7.5f) show an increase in KAM value, with values of 1.13° and 1.2°, respectively, indicating an increase in dislocation density in both phases.

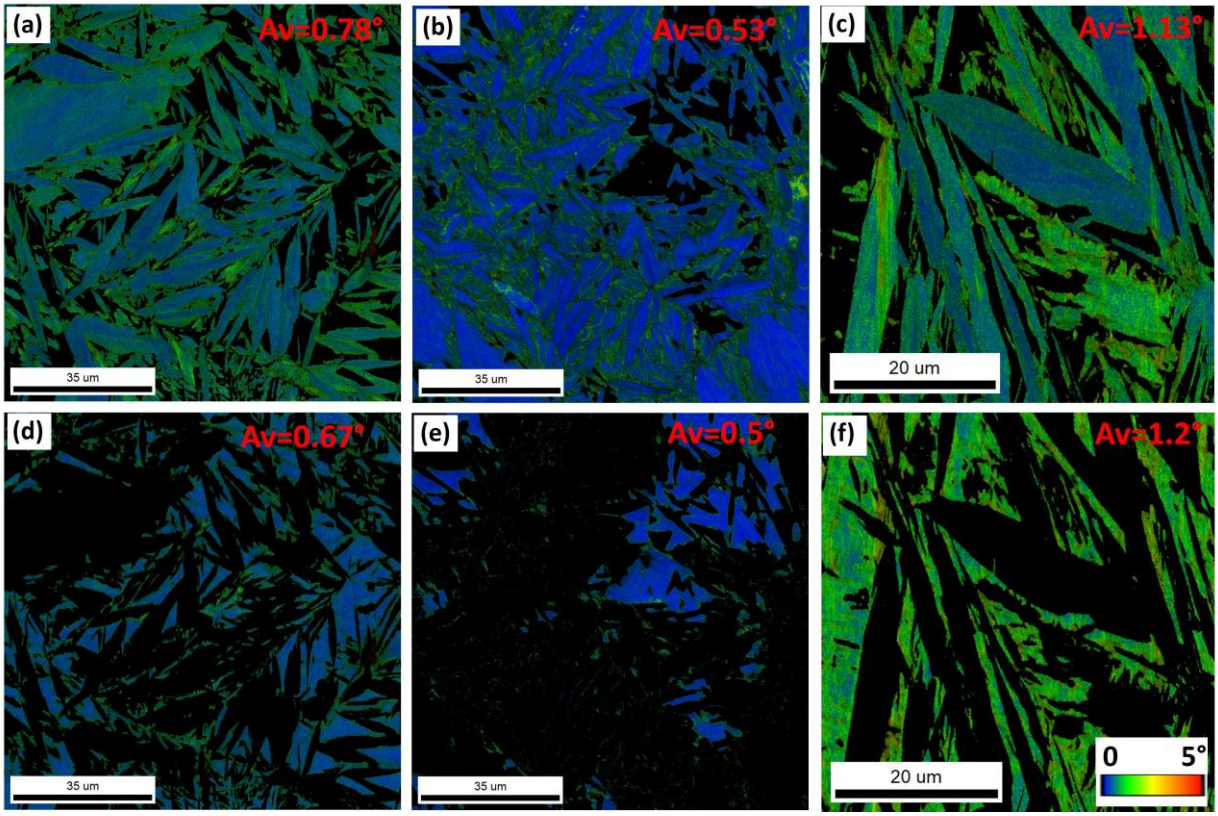

Figure 7.5. *KAM map of martensite phase (a) D2-A, (b) D2-A-EP-1 and (c) D2-A-EP-1-LCD and austenite phase (d) D2-A, (e) D2-A-EP-1 and (f) D2-A-EP-1-LCD samples.*

X-ray diffraction peak analysis of the D2-A sample (Figure 7.6a) reveals the presence of austenite along with the tetragonal martensite phase, indicated by peak splitting of (111), (200), and (211) peaks. The magnified region does not show any distinct carbide peaks, but their presence is likely, as their most intense peaks are positioned near the same Bragg angle of martensite and austenite phases. After electropulsing (D2-A-EP-1), additional phases

are formed (as seen in the magnified region) and they match with the d-spacings of cementite, as shown in Figure 7.6b. Moreover, the intensity of the austenite phase decreases, while that of martensite phase increases, indicating the formation of additional martensite/bainite after electropulsing treatment. In the D2-A-EP-1-LCD sample (Figure 7.6c), the intensity of the austenite peak is not significantly decreased, but from the integrated intensity, it is found that more martensite/bainite is formed compared to the D2-A sample. There is also no significant carbide precipitation observed in this case. The tetragonality of the peaks is confirmed by comparing the peak positions with those of the directly water-quenched (WQ) sample, which clearly shows peak splitting due to the tetragonality of martensite.

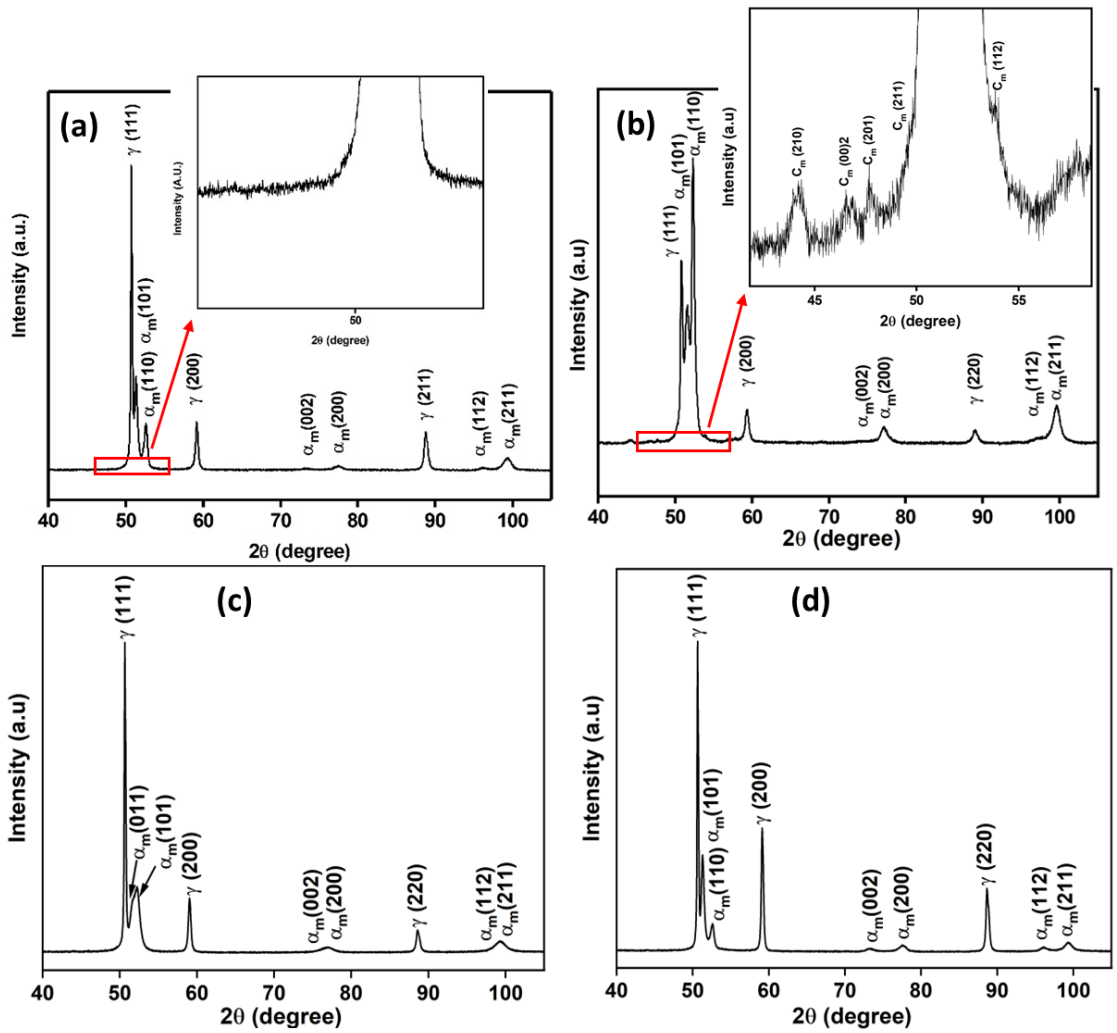

Figure 7.6. *XRD peaks of (a) D2-A, (b) D2-A-EP-1, (c) D2-A-EP-1-LCD and (d) D2-M samples.*

The lattice parameter of austenite, determined using the Rietveld refinement method, shows a decrease in value from 3.618 Å to 3.612 Å after electropulsing (D2-A-EP-1). However, when a low current density is applied, the lattice parameter is increased to 3.622 Å (Table 7.1). Comparing with the WQ sample, it shows a lattice parameter of 3.62 Å, and the carbon content in the RA is calculated to be 1.04 mass% in this case. For the air-cooled sample (D2-A), the carbon content is calculated to be 1.02 mass%, which reduces to 0.9 mass% after electropulsing at higher current density and increases further to 1.11 mass% after electropulsing at lower current density. The c/a ratio is highest for the WQ sample (1.05), followed by the air-cooled, electropulsed at high current density, and electropulsed at low current density samples (Table 7.1).

Table 7.1. XRD peak profile analysis

Sample	Austenite lattice parameter (Å)	Carbon content in retained austenite (mass%)	c/a
D2-A	3.618	1.02	1.04
D2-A-EP-1	3.612	0.9	1.03
D2-A-EP-1-LCD	3.622	1.11	1.01
D2-M	3.62	1.04	1.05

The TEM-BF image of the air-cooled sample (D2-A) reveals the presence of the martensite phase (Figure 7.7a), which is also confirmed in the corresponding diffraction pattern (DP). Another region of the D2-A sample shows a midrib in the lenticular martensite (Figure 7.7b) along with twins. The twins originate from the midrib and it is disapperared before the martensite boundary. A magnified BF region shows midrib along with precipitation of carbides as shown in Figure 7.7c. The corresponding DP shows spots from two different zone axes of the martensite, namely [012] and [111] (Figure 7.7d). The DF image corresponding to a spot of the [111] zone axis shows the midrib of the martensite with the presence of fine carbides (Figure 7.7e), and another DF image corresponding to a spot of the [012] zone axis represents

the rest of the martensite region with some fine carbides (Figure 7.7f). The drawn in light blue colour in the DP (Figure 7.7d) belongs to the carbide phase, which is observed in both the dark-field images. The martensite is formed by air cooling and the dwell at the temperature range of its formation is sufficient for tempering to occur. Therefore, it leads to the precipitation some amount of cementite as observed in Figure 7.7f.

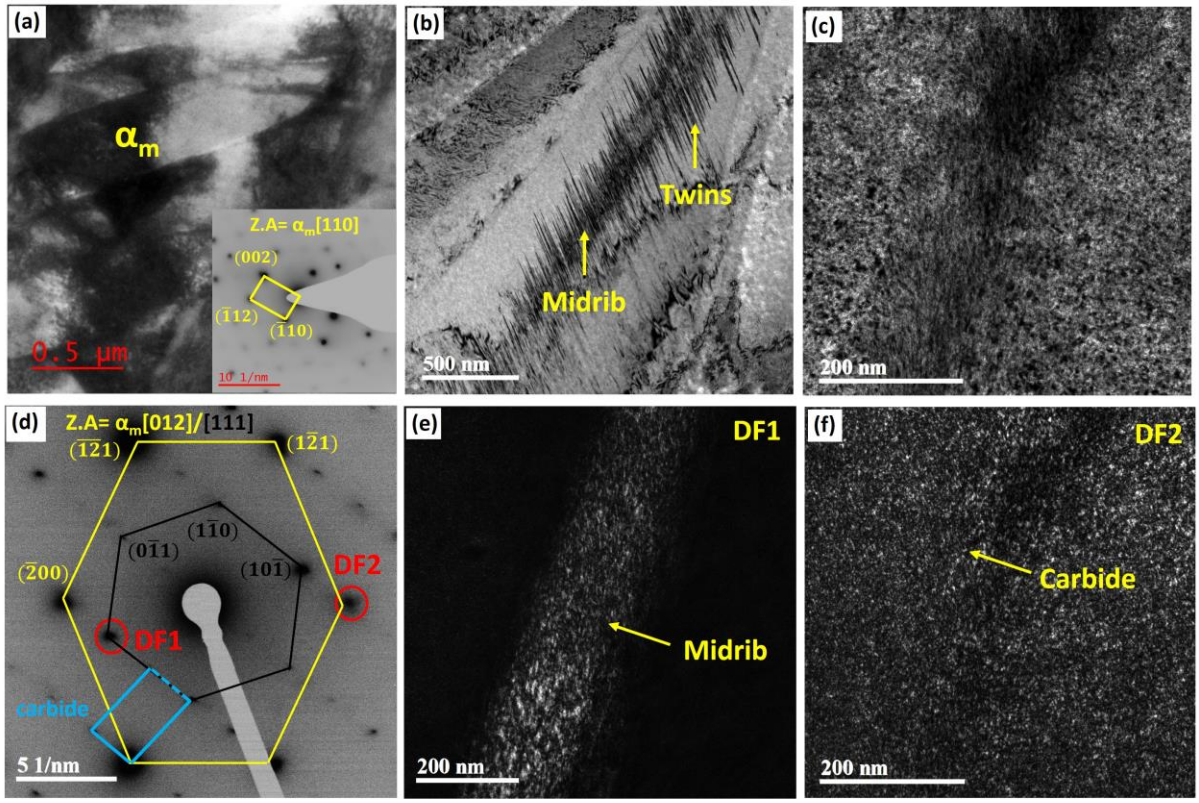

Figure 7.7. *TEM images of D2-A sample (a) BF and corresponding DP, (b) BF image showing midrib in a lenticular martensite, (c) magnified BF region, (d) corresponding DP, (e and f) DF taken from indicated regions of DP in Figure d showing midrib and carbides in matrix phase respectively.*

After EP of the D2-A sample (D2-A-EP-1), there is precipitation of carbides in both the martensite and the austenite phases, as shown in the bright-field (BF) image in Figure 7.8a and the DF image in Figure 7.8b. Another BF image of RA (Figure 7.8c) shows transformation into martensite, which is also confirmed in the selected area diffraction pattern in Figure 7.8d.

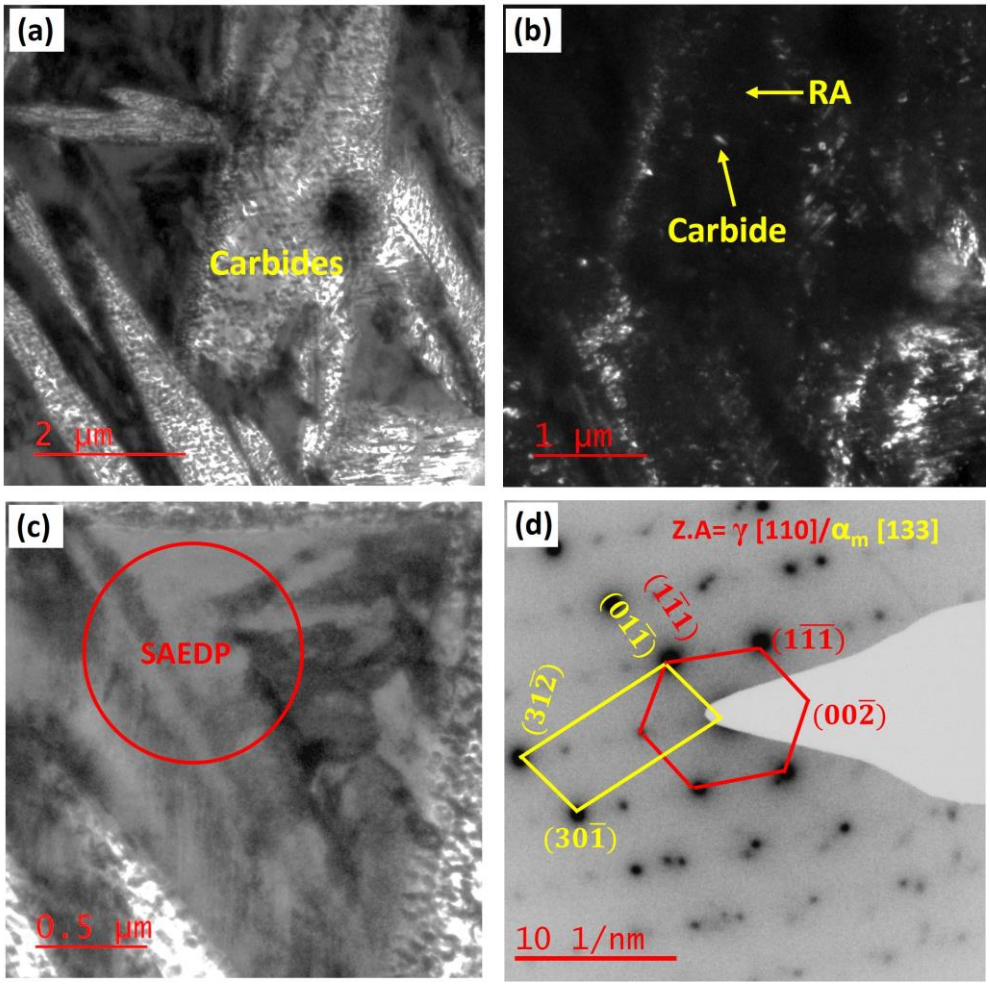

Figure 7.8. *TEM images of D2-A-EP-1 sample (a) BF, (b) DF (c) BF image of RA and (d) SAEDP corresponding to position circled in the BF image of Figure c.*

In the D2-A-EP-1-LCD sample, a region with retained austenite in the TEM-BF image displays the formation of twin martensite of different variants (Figure 7.9a). A closer examination of the twin region in the BF image and its corresponding DP also confirms the presence of martensite (Figure 7.9b). The DF image taken from the spot marked in the DP shows the coexistence of some carbides along with twin martensite (Figure 7.9c). These carbides may have been inherited from the base D2-A sample. To further understand the changes within the martensite phase, another BF image is analysed (Figure 7.9d). The corresponding DP (Figure 7.9e) reveals the presence of both austenite and martensite phases. The DF image (Figure 7.9f) corresponding to the spot in Figure 7.9e shows the presence of martensite without significant carbide precipitation.

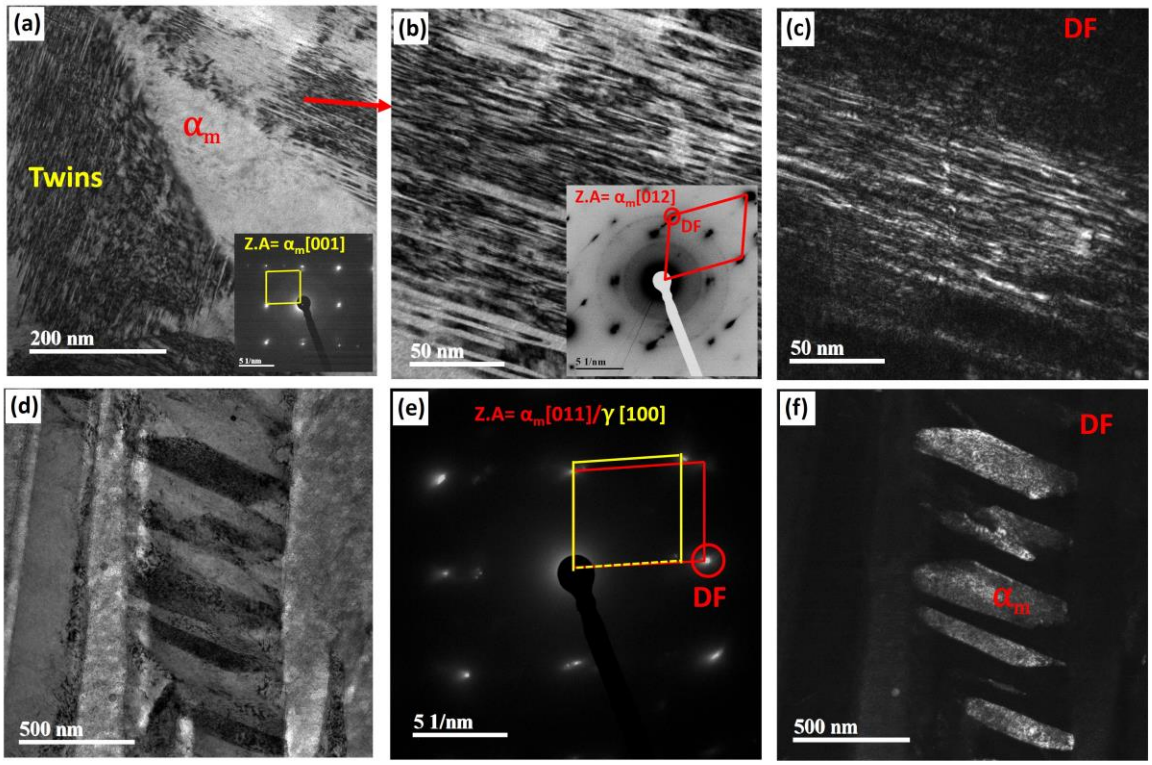

Figure 7.9. *TEM images of D2-A-EP-1-LCD sample (a-c) BF, (d) DP corresponding to Figure c (e, f) DF images corresponding position 1 and 2 in the DP of Figure 7.9d.*

The hardness and elastic modulus of the samples are determined by applying a 5000 mN force using an instrumented hardness testing machine. The applied force versus indentation depth plot is depicted in Figure 7.10. In the D2-A sample, there is continuous depth of indentation up to 2.2 µm, after which discontinuous bursts are observed, as indicated by the arrow marks. On the contrary, both the D2-A-EP-1 and D2-A-EP-1-LCD samples display a continuous curve throughout the loading process.

The Vickers hardness value of the D2-A sample is measured to be 557±20 HV, which increases to 629±12 HV after EP at higher current density (D2-A-EP-1). Notably, the D2-A-EP-1-LCD sample demonstrates a significant increase in hardness value to 708±29 HV. Meanwhile, the elastic modulus value undergoes a decrease, reducing from 174±3 GPa in the D2-A sample to 172±2 GPa in D2-A-EP-1. The application of EP at low current density (D2-A-EP-1-LCD), where no significant carbide precipitation is observed, results in a substantial reduction of the elastic modulus to 137±3 GPa (Table 7.2).

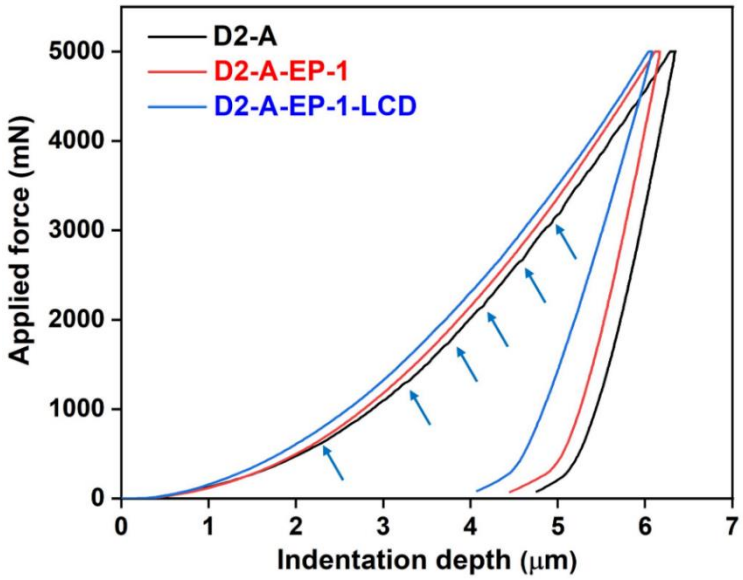

Figure 7.10. *Applied force vs. indentation depth plot*

Table 7.2. Results of instrumented hardness testing

Sample	Instrumented Hardness (HV)	Instrumented elastic modulus (GPa)
D2-A	557±20	174±3
D2-A-EP-1	629±12	172±2
D2-A-EP-1-LCD	708±29	137±3

7.3 Discussion

The alteration of microstructure and phase transformation that occurs during electropulsing is thought to result from a combination of both thermal and athermal effects, as elucidated in previous chapters. This combined influence also contributes to the modified outcomes and adjustments in hardness behaviour. The subsequent analysis shows microstructural transformations within each phase and their corresponding discussion.

7.3.1 Stability of martensite

The martensite morphology resulting from air-cooling of high-carbon low alloy steel takes a lenticular shape with a midrib in between. This midrib constitutes a plate-like martensite

structure [237], a feature that is also confirmed in the TEM DP presented in Figure 7.7d. The [012] zone axis corresponds to lenticular martensite (Figure 7.7f), while the [111] zone axis corresponds to the midrib of the lenticular martensite (Figure 7.7e).

The initial carbon content in the alloy is about 1.06 mass%, which is sufficient to induce tetragonality in the martensite. The carbon content required for the tetragonality in the martensite is about 0.2 mass% [238]. The calculated mass% of carbon in the austenite phase of WQ sample is about 1.04 mass%, due to some error in calculation or minor decarburization during heat treatment. The WQ sample is expected to retain all the carbon initially present within the austenite phase. This is further supported by the higher tetragonality (c/a = 1.05) observed in the WQ sample compared to the other one. However, in the case of air-cooled sample (D2-A), the tetragonality is decreased (c/a=1.04) and also the mass% of carbon in RA.

During air-cooling, there is a concurrent diffusion of carbon into the RA phase. However, carbide precipitation is evident in TEM micrographs (Figure 7.7e, f), leading to some degree of carbon depletion. Following electropulsing (EP) at high current density, carbon content in the martensite decreases further due to carbide precipitation, ultimately resulting in a reduced tetragonality. Surprisingly, the low current density sample (D2-A-EP-1-LCD) exhibits a lower c/a value compared to the D2-A-EP-1 sample, despite greater carbide precipitation in the latter.

This discrepancy can be attributed to two potential factors: firstly, decarburization during the heat treatment process, and secondly, Zener ordering [239,240]. Substantial tetragonality necessitates carbon atoms to be positioned in specific sites, thereby enhancing the ordering effect. In contrast, a disordered arrangement of carbon atoms positioned in all sites would result in reduced effective strain, leading to diminished tetragonality [239].

The formation of cementite within martensite of the D2-A-EP-1 sample, as observed in XRD pattern (Figure 7.6b), is mainly due to the combined thermal and athermal effects of EP, as

discussed earlier. When considering only the thermal effect, it leads to the formation of very fine cementite, as seen in the D2-A sample (Figure 7.7f). This observation is further supported by precipitation simulations in Chapter 6. This phenomenon has also been noted in earlier research [145], wherein the accelerated nucleation rate during EP is highlighted as a substantial contributing factor.

In the case of the D2-A-EP-1-LCD sample, the limited carbide precipitation can be attributed to the lower current density and resulting temperature rise (290°C) compared to the D2-A-EP-1 sample. The interaction of EP parameters and thermal effects plays a critical role in determining the resulting carbide morphology and distribution, affecting the material's microstructure and properties.

7.3.2 Transformations in retained austenite

In the previous chapter, the electropulsing-induced transformation of the austenite phase was investigated. In this context, the major phase formed was bainite, with additional bainite formation observed near the sheaves, and martensite primarily in the blocky retained austenite. Compared to the earlier case, the carbon content in the RA phase here is lower, and there is no additional strain generated within the RA phase, which was present previously due to dislocation generation.

The SEM SEI (Figure 7.2c) confirms the additional martensite formation from the RA phase in the D2-A-EP-1 sample. In this micrograph, the martensite (α_m) that existed before electropulsing precipitates cementite, resulting in decreased strain and proper etching. On the other hand, the freshly formed martensite (α'_m), containing a higher amount of carbon and exhibiting higher strain and inadequate etching does not precipitate cementite (Figure 7.2c). The formation of martensite in electropulsed materials is also aided by the decrease in elastic modulus, as observed in the instrumented hardness testing (Table 7.2). Similar observations

are made in the D2-A-EP-1-LCD sample, where the temperature rise is only ≈290°C and no significant carbide precipitation occurs (Figure 7.9a). Thus, the formation of thermally induced martensite is absent, indicating that martensite formation is primarily due to the athermal effect of electropulsing.

Confirmation of bainite (α_b) formation from the RA phase is also obtained from the SEM SEI image in Figure 7.2c. This image reveals two distinct categories of martensite, as discussed earlier. Meanwhile, deeply etched plate-shaped structures without carbide precipitation correspond to bainite. Indirect confirmation of bainite formation is evident from the KAM map of the D2-A-EP-1-LCD sample, where additional dislocations are generated in the austenite phase. In situations involving bainite formation, dislocations are predominantly generated in the RA phase [82]. Additionally, the measurement of carbon content in the RA phase using XRD provides further insight into bainite formation. The relatively high carbon content (1.11 mass%) in the RA phase confirms the occurrence of bainite phase formation. This is consistent with the rejection of carbon into austenite after the formation of a bainite plate.

7.3.3 Changes in hardness after electropulsing

The D2-A sample comprises a significant fraction of the soft austenite phase, alongside martensite. The force vs. depth of indentation curve during loading exhibits a discontinuous burst due to strain-hardening behaviour. This behaviour can be attributed to the interaction of dislocations or the strain-induced martensitic transformation [241]. The initial bursts result from dislocation generation and pile-up, while in later stages, the dominance of transformation into the martensite phase is observed. However, in electropulsed samples, most of the RA phase transforms into bainite/martensite, eliminating the strain-hardening effect. Consequently, the force vs. depth of indentation curve appears continuous without exhibiting bursts.

The Vickers hardness value is notably higher in the D2-A-EP-1-LCD sample, where a smaller amount of bainite/martensite transformation is observed compared to the D2-A-EP-1 sample. The higher temperature rise in the D2-A-EP-1 sample leads to some softening behaviour due to dislocation and boundary movements. The presence of newly formed carbide precipitates also contributes to a lower carbon content in the martensite phase. In contrast, in the D2-A-EP-1-LCD sample, additional strain is generated in both phases due to bainite/martensite formation, and no significant recovery is observed due to the lower temperature rise.

From this it is concluded that in martensite-austenite phase with low alloy steel, electropulsing primary contribute towards the enhancement of hardness.

7.4 Conclusions

- Air-cooling of high carbon low alloy steel sample results in tetragonal martensite and retained austenite. There are some amount of cementite within martensite due to tempering.
- The boundary between martensite and retained austenite is primarily low-angle in nature. On electropulsing, significant part of these boundaries converts into high-angle boundaries through migration.
- Electropulsing, results in the transformation of retained austenite in to good amount of martensite as well as some amount of bainite.
- The extent of this transformation increases with higher current density during electropulsing.
- Electropulsing at high current density induces the precipitation of carbides within both the martensite and retained austenite phases.
- Hardness of the electropulsed sample increases due to additional bainite/martensite formation and it is more in case of low current density sample where temperature effect is less for softening.